Marine and Petroleum Geology 112 (2020) 104068

Contents lists available at ScienceDirect

Marine and Petroleum Geology

journal homepage: www.elsevier.com/locate/marpetgeo

Research paper

Variability of rock mechanical properties in the sequence stratigraphic context of the Upper Devonian New Albany Shale, Illinois Basin

Bei Liu[a,*], Juergen Schieber[a], Maria Mastalerz[b], Juan Teng[b,c]

[a] Department of Earth and Atmospheric Sciences, Indiana University, Bloomington, IN, 47405, USA
[b] Indiana Geological and Water Survey, Indiana University, Bloomington, IN, 47405-2208, USA
[c] College of Energy, Chengdu University of Technology, Chengdu, Sichuan, 610059, China

ARTICLE INFO

Keywords:
Hardness
Brittleness index
Devonian black shales
Sequence stratigraphy
Biogenic quartz
Shale reservoir
New Albany Shale

ABSTRACT

Rock mechanical properties of tight shale reservoirs are important parameters in the exploration and development of unconventional shale oil and gas. Understanding the stratigraphic variability of rock mechanical properties in black shale successions is important for identifying promising intervals for hydraulic stimulation. High-resolution hardness tests (6 cm spacing) with an Equotip Bambino 2 hardness tester were conducted on a New Albany Shale core to study the stratigraphic variability of rock mechanical properties. Combined with high-resolution geochemical analyses (8 cm spacing) acquired with a portable X-ray fluorescence spectrometer, it is possible to relate hardness variability to shale composition.

The results of our study suggest an average quartz content of about 28% for the entire succession. Approximately half of that amount (13%) is interpreted to be of biogenic origin. Biogenic quartz, mainly derived from dissolution of radiolaria, occurs as authigenic quartz precipitated in *Tasmanites* cysts, and as microcrystalline quartz precipitated in the shale matrix. Petrographic observations indicate that the hardness of the New Albany Shale is critically controlled by biogenic quartz content, not by total quartz content as suggested in multiple prior studies. Biogenic quartz forms an interconnected stiff framework which increases the hardness of shales. In contrast, dispersed "hard" grains (e.g., detrital quartz, feldspar, and dolomite) do not contribute to brittle behavior. When examined under a scanning electron microscope, "hard" shales are rich in biogenic quartz and contrast visibly with "soft" shales that are characterized by high contents of clay minerals. Negative correlation between hardness and Al_2O_3 content, as well as differential compaction of clay minerals around "hard" grains, indicate that clay minerals are an important ductile component in the New Albany Shale. Although the general softness of kerogen suggests that there should be an influence of organic matter on hardness, this effect is counteracted by biogenic quartz cementation which has a comparable stratigraphic distribution pattern. We propose a new mineral-composition-based brittleness index on the basis of biogenic quartz content to characterize the brittleness of tight shale reservoirs.

Within a sequence stratigraphic context, the hardness of the New Albany Shale increases in transgressive systems tracts, reaches a maximum at maximum flooding surfaces, and decreases in highstand systems tracts with the exception of the Blocher Member. Maximum flooding surface intervals have the highest potential to develop brittle fractures and should be potential targets for hydraulic stimulation.

1. Introduction

Rock mechanical properties are important parameters in unconventional petroleum systems because they not only control the development of natural fractures in tight shale reservoirs, but also determine how shales respond to hydraulic stimulation (Gale et al., 2007, 2014; Grieser and Bray, 2007; Wang and Gale, 2009). Young's modulus and Poisson's ratio are two key parameters that are commonly used to characterize the mechanical properties of rocks (Rickman et al., 2008; Wang and Gale, 2009; Bustin and Bustin, 2012; Labani and Rezaee, 2015). Generally speaking, high Young's modulus and low Poisson's ratio indicate a high degree of rock brittleness, whereas rocks having low Young's modulus and high Poisson's ratio are considered ductile (Rickman et al., 2008; Wang and Gale, 2009; Labani and Rezaee, 2015).

Young's modulus and Poisson's ratio of rocks can be determined in the laboratory or can be derived from geophysical logs (Rickman et al.,

* Corresponding author.
E-mail address: liubei@iu.edu (B. Liu).

https://doi.org/10.1016/j.marpetgeo.2019.104068
Received 10 March 2019; Received in revised form 11 August 2019; Accepted 30 September 2019
Available online 01 October 2019

2008; Labani and Rezaee, 2015). Hardness testing with rebound hammers (Schmidt hammer) is yet another approach to characterize the rock mechanical properties of rocks (Lee et al., 2014, 2016; Ritz et al., 2014; Ghanizadeh et al., 2015; Yang et al., 2015; Dong et al., 2017, 2018). High hardness generally indicates high Young's modulus and low Poisson's ratio, and high brittleness of shales (Dong et al., 2017, 2018).

Rock mechanical properties of black shales are fundamentally controlled by mineralogical composition (Walles, 2004; Jarvie et al., 2007; Wang and Gale, 2009; Aoudia et al., 2010; Passey et al., 2010; Sondergeld et al., 2010; Sone and Zoback, 2013a,b; Labani and Rezaee, 2015; Dong et al., 2017, 2018), organic matter content (Walles, 2004; Aoudia et al., 2010; Eliyahu et al., 2015; Labani and Rezaee, 2015), and also thermal maturity (Wang, 2008; Labani and Rezaee, 2015; Dong et al., 2018). Quartz and carbonate minerals are generally considered to be brittle minerals (Jarvie et al., 2007; Wang and Gale, 2009; Dong et al., 2018), whereas clay minerals and organic matter are commonly thought to be ductile components in black shales (Walles, 2004; Jarvie et al., 2007; Wang and Gale, 2009; Aoudia et al., 2010; Passey et al., 2010; Kumar et al., 2012; Zargari et al., 2013; Eliyahu et al., 2015; Labani and Rezaee, 2015; Dong et al., 2017, 2018; Li et al., 2018a,b). Because mineral and organic matter composition vary stratigraphically, the rock mechanical properties of shales vary stratigraphically as well, i.e., some intervals are more easily fractured during hydraulic stimulation than others (Jarvie et al., 2007). This stratigraphic variability can be related to depositional and diagenetic processes that are in turn linked to fluctuations of relative sea level (Harris et al., 2011; Lash and Blood, 2011; Slatt and Abousleiman, 2011; Liu et al., 2018). For example, Slatt and Abousleiman (2011) reported three orders of stratigraphic brittle-ductile couplets resulting from relative sea-level fluctuations in the Barnett Shale.

The Upper Devonian New Albany Shale (NAS) of the Illinois Basin has high organic matter content, ranging from < 1% to 20 wt. % total organic carbon (TOC) content (Chou et al., 1991), with an average TOC of 6.53 wt. % (Liu et al., 2019). The thermal maturity of the NAS is dominantly within the early oil window but has reached vitrinite reflectance (R_o) 1.5% in the Hicks Dome area of Hardin County, Illinois (Strąpoć et al., 2010; Mastalerz et al., 2013). Estimates of shale gas-in-place and recoverable natural gas in the NAS range from 86–160 trillion cubic feet (2.44–4.53 trillion cubic meters) and 1.30–8.12 trillion cubic feet (36.81–229.93 billion cubic meters), respectively (Hill and Nelson, 2000; Swezey, 2007). Commercial gas production from the NAS started in the late 1800s and initial potential of wells drilled in the NAS ranges from 57–124594 m^3/day with an average value of 5295 m^3/day (Hamilton-Smith et al., 1994). Natural gas produced from the NAS is considered a mixture of thermogenic and biogenic methane (Martini et al., 2008; Strąpoć et al., 2010). Besides being a producer of natural gas, the NAS also produces oil where it lies within the oil window (Nuttall et al., 2015).

The overall goal of this investigation is to study the rock mechanical properties of the NAS and see if it may provide insights into developing the NAS as a shale oil play. Specifically, this study aims to (1) document the stratigraphic variability of rock mechanical properties of the NAS; and (2) study the control of shale composition (quartz, calcite, dolomite, clay minerals, and organic matter) on the mechanical properties of black shales within the NAS succession.

2. Geological setting

The Illinois Basin is a cratonic basin located across what are now central and southern Illinois, southwestern Indiana, and western Kentucky (Heidlauf et al., 1986, Fig. 1). It is separated from the Appalachian Basin by the Cincinnati Arch (Buschbach and Kolata, 1990, Fig. 1). The NAS, a marine black shale unit, was deposited during the Late Devonian when the Illinois Basin was covered by epicontinental seas (Lineback, 1964, 1968; Beier and Hayes, 1989) and thins eastward towards the Cincinnati Arch (Lazar, 2007). It is time-equivalent with the Ohio Shale, the Antrim Shale, the Chattanooga Shale, and the Bakken Shale in North America (Schieber, 1998; Schieber and Lazar, 2004). Lithologically, it is composed of black to brownish laminated to banded shales with interbedded greenish-gray bioturbated shales with indications of bottom-current activity and multiple styles and intensities of bioturbation (Lineback, 1964, 1968; Beier and Hayes, 1989; Schieber and Lazar, 2004; Lazar, 2007).

The NAS overlies the Middle Devonian North Vernon Limestone and is unconformably overlain by the Falling Run Bed, a phosphatic lag deposit sourced from reworked NAS (Campbell, 1946; Schieber and Lazar, 2004). Its five members are, in ascending order, the Blocher, Selmier, Morgan Trail, Camp Run, and Clegg Creek Members (Lineback, 1964, 1968) and can be subdivided into four basin-wide depositional sequences (Schieber and Lazar, 2004; Lazar, 2007).

3. Materials and analytical methods

3.1. Samples

A NAS core from Daviess County, Indiana, USA (Fig. 1) was selected to study the stratigraphic variability of rock mechanical properties. The core (well name: 1-3 Kavanaugh) was drilled in 1994 by Deka Exploration Inc. Its coordinates are X = 494611, Y = 4276705 (North American Datum 83; Lazar, 2007). It is 39.43 m thick and has a R_o value of 0.55%, indicating early maturity. Sequence stratigraphic and geochemical studies of this core have been presented in Lazar (2007) and Liu et al. (2019).

3.2. Portable X-ray fluorescence spectroscopy

Portable x-ray fluorescence (pXRF) spectroscopy is fast and non-destructive, and has been applied in mudrock geochemistry (Rowe et al., 2012). A Thermo Niton XL3t GOLDD + spectrometer was used to measure elemental composition at a spacing of about 8 cm (11 mm diameter analysis spot, 75 s analysis time) on cleaned core slabs. The pXRF spectrometer was run in “Test All Geo” mode, and at the beginning and end of each analytical session, three USGS reference materials (SDO-1 [shale], SBC-1 [shale], and COQ-1 [carbonatite]) were analyzed to validate precision and accuracy of the analyses (McLaughlin et al., 2016).

Because pXRF spectrometry lacks the high detection accuracy of standard XRF spectrometry on fused glass discs, the elements silicon (Si), aluminum (Al), calcium (Ca), and magnesium (Mg) contents were calibrated to standard XRF data obtained from seventeen NAS samples (Fig. 2) previously analyzed by Lazar (2007). Analyses were conducted at the same depths and exact same locations where these 17 samples were cut from the core. The calibration of Si and Al was presented in Liu et al. (2019). The analysis errors for Si, Al, Ca, and Mg are 0.78%, 2.88%, 4.02%, and 26.67%, respectively. The high analysis error for Mg could be due to its low content.

The contents of major element oxides (SiO_2, Al_2O_3, CaO, and MgO) were calculated from Si, Al, Ca, and Mg concentrations after calibration. Because Si is primarily associated with quartz and clay minerals (mostly illite) in the NAS, the content of total quartz was calculated using the equation below (Eq. (1)):

$$\text{Quartz} = [\text{Si}_{\text{sample}} - [(\text{Si/Al})_{\text{illite}} \times \text{Al}_{\text{sample}}]] \times 60/28 \quad (1)$$

Where 60 and 28 are the molar masses of SiO_2 and Si, respectively. A Si/Al ratio of 1.65 was used as the Si/Al ratio of pure illite (Ylagan et al., 2000). Although albite and potassium feldspar with a higher Si/Al ratio exist in the NAS, their contents are generally low and do not significantly affect the Si/Al ratio of bulk analyses.

Biogenic quartz (termed bioquartz for the remainder of this paper) was precipitated from pore waters that had become supersaturated because of prior dissolution of biogenic opal (Schieber, 1996; Schieber

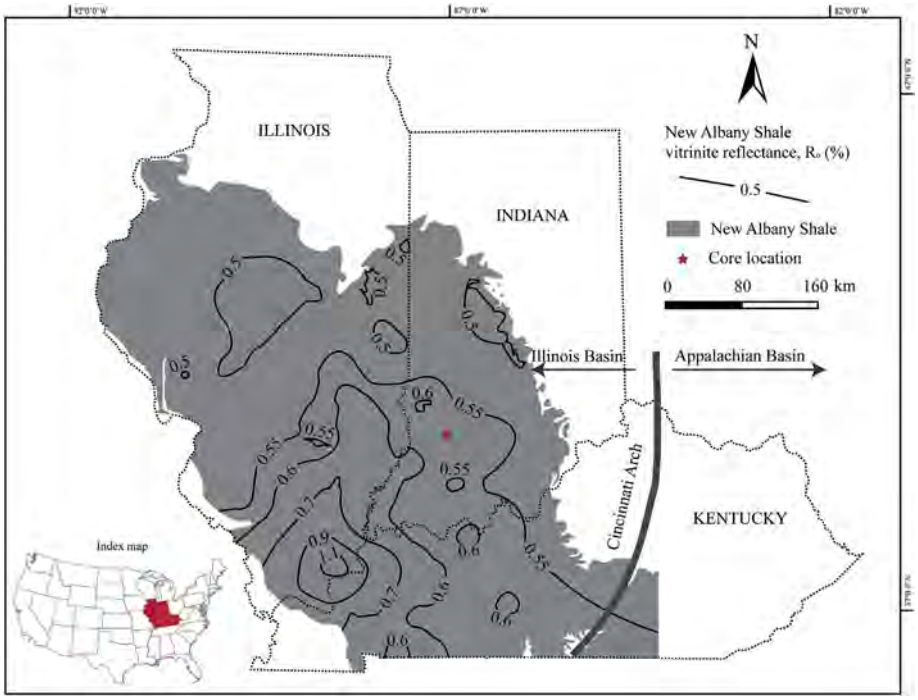

Fig. 1. Map showing the location of the drill core and the extent of the NAS. Modified from McFarlan (1943) and Mastalerz et al. (2013).

et al., 2000) and its content was calculated by subtracting the Si associated with detrital Al from total Si, following a formula (adjusted for oxides) provided by Ross and Bustin (2009):

$$\text{Bioquartz} = [\text{Si}_{\text{sample}} - [(\text{Si/Al})_{\text{background}} \times \text{Al}_{\text{sample}}]] \times 60/28 \quad (2)$$

A Si/Al ratio of 2.55 was used as the detrital background value, because it is the lowest Si/Al ratio measured in the NAS (Liu et al., 2019). SEM examination of shale samples from core intervals with this Si/Al ratio mainly shows detrital materials and diagenetic bioquartz (from dissolution of radiolaria) is rare or absent (Liu et al., 2019).

3.3. Hardness tests

An Equotip Bambino 2 hardness tester was used to measure the hardness of the 1-3 Kavanaugh core at an approximate spacing of 6 cm. Although originally developed for measuring the hardness of metals, the Equotip hardness tester has been employed to characterize the mechanical properties of black shales in several recent studies (Lee et al., 2014, 2016; Ritz et al., 2014; Ghanizadeh et al., 2015; Yang et al., 2015; Dong et al., 2017, 2018; Stewart, 2017). Hardness testing with the rebound method can provide fast, non-destructive, quantitative, and high-resolution measurements of rock mechanical properties that compare favorably traditional laboratory tests (Lee et al., 2014, 2016; Yang et al., 2015).

During hardness measurements, a small tungsten carbide ball is launched by spring energy against the core slab and then the ball rebounds after impacting the rock surface (Ritz et al., 2014). The Leeb hardness value (HL) is defined as the ratio of the rebound velocity to the impact velocity multiplied by 1000 (Ritz et al., 2014). A schematic diagram of the Equotip hardness tester can be found at Lee et al. (2016). The core slab was placed on a V-shape metallic mold to make sure the slab was stable during the measurement (Fig. 3). At least five measurements were taken at each depth and these measurements were averaged to yield an average hardness value for each depth. All measurements were concentrated near the center of the core slab to avoid movement of the slab. Fractures were avoided during the measurement.

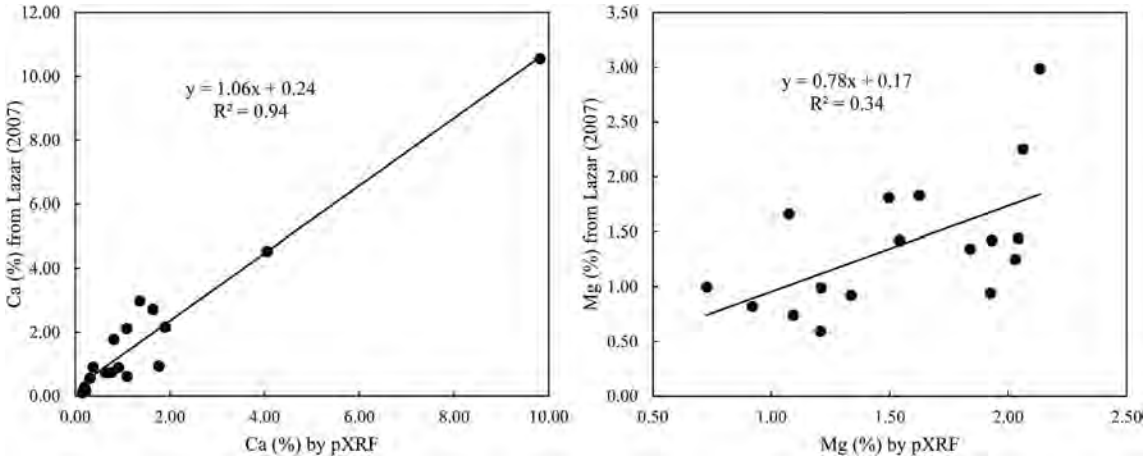

Fig. 2. Relationships between Ca and Mg content obtained by a pXRF analyzer and Ca and Mg content reported for the same 17 NAS samples by Lazar (2007). Although the 17 measurements are from samples at the same depth, they are not identical samples, which may cause some scatter of the data points.

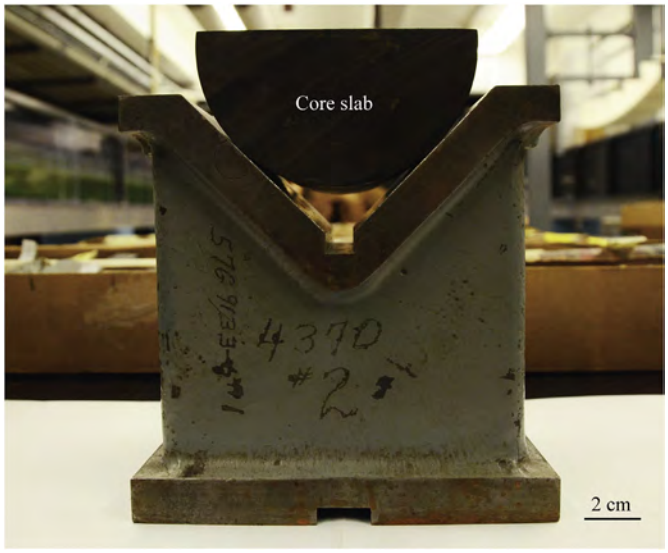

Fig. 3. Side view of the metallic mold used for hardness tests of the NAS core.

3.4. Scanning electron microscope petrography

Petrographic characteristics of shale samples having high and low hardness values were examined using a field-emission scanning electron microscope (SEM) (FEI Quanta 400 FEG) in low vacuum mode. The accelerating voltage was 15 kV and the working distance was approximately 10 mm.

4. Results

4.1. Major element oxides

Total quartz content in the 1-3 Kavanaugh core, as derived via Eq. (1), ranges from 8.73 to 78.14% with an average content of 27.64%, out of which from 0 to 75.29% (average 12.88%) is considered of biogenic origin (as derived via Eq. (2)). On average, bioquartz accounts for approximately 47% of total quartz. The Clegg Creek Member (sequence 4; Fig. 4) has a total quartz and bioquartz content of 33.17% and 20.38%, respectively, with bioquartz accounting for about 61% of total quartz. The observation that total quartz and bioquartz show a similar stratigraphic distribution pattern (Fig. 4) suggests a significant biogenic input to the quartz content of the NAS. Al_2O_3 content ranges from 0 to 19.26% with an average content of 14.45%. CaO and MgO contents range from 0.47 to 56% (average 3.08%) and 0 to 7.98% (average 2.29%), respectively. The lower half of the Blocher Member exhibits high CaO (average 11.28%) and MgO (average 3.06%) contents compared to the rest of the core (Fig. 4). In most cases, CaO content covaries with MgO content (Fig. 4), suggesting that most Ca is associated with dolomite. The mineralogical compositions of the NAS as derived from pXRF analyses are comparable to results from X-ray diffraction studies (Frost and Shaffer, 1994; Mastalerz et al., 2013, 2016).

4.2. Stratigraphic variability of hardness

The Leeb hardness values of the 1-3 Kavanaugh core range from 432 to 788 with an average value of 526. The Clegg Creek Member has the highest hardness (average 565), whereas the average hardness of the rest of the core is only 509. Within a sequence stratigraphic context, hardness increases in transgressive systems tracts (TSTs), reaches a maximum at maximum flooding surfaces (MFSs), and decreases in highstand systems tracts (HSTs) with the exception of the Blocher Member (Fig. 4). Stratigraphically, the hardness profile shows a similar distribution pattern to the bioquartz profile, and an inverse pattern when compared to the Al_2O_3 profile (Fig. 4).

4.3. Petrographic characteristics

Hardness values of the studied core reach a maximum (average 630) at the MFS interval of the Clegg Creek Member (Fig. 4). Shales in this interval contain high abundances of authigenic quartz and pyrite (Fig. 5). Bioquartz accounts for approximately 30% of the shale composition. Bioquartz occurs as authigenic quartz precipitated in algal cysts (Fig. 5A – E), and as microcrystalline quartz precipitated in the

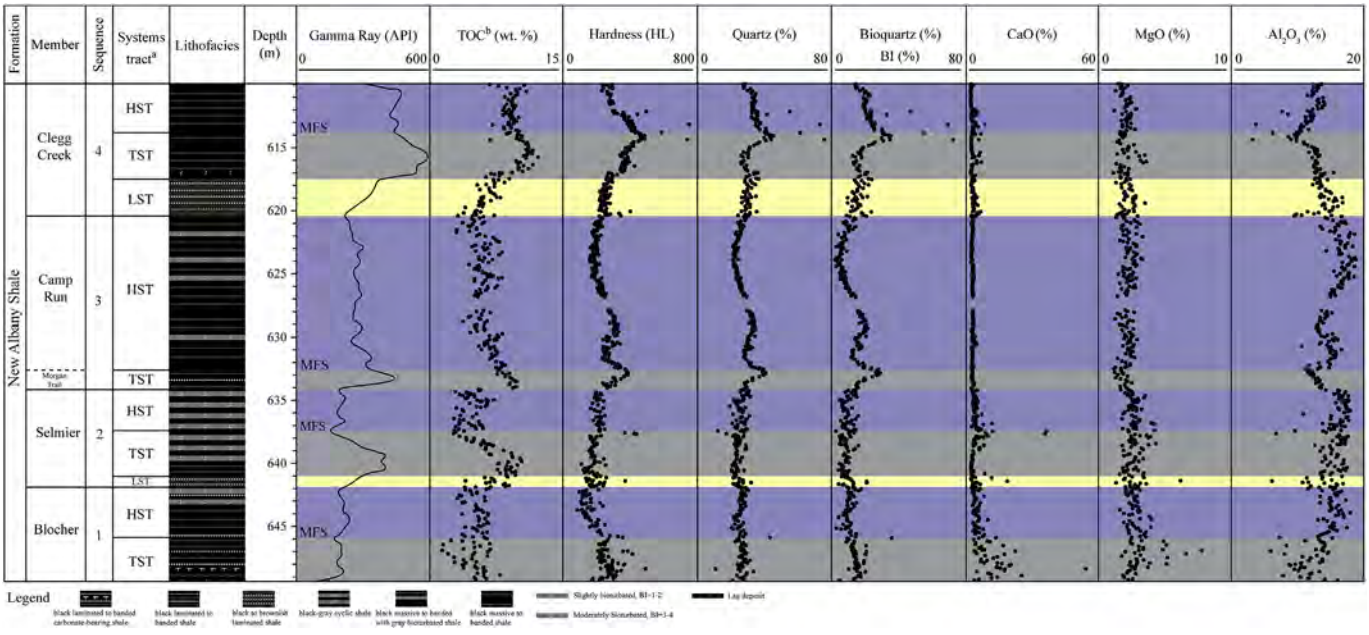

Fig. 4. Stratigraphic distribution of lithofacies, gamma-ray intensity, total organic carbon (TOC) content, hardness value, total quartz, bioquartz, CaO, MgO, and Al_2O_3 content, and brittleness index (BI) for the studied NAS core. Interval from 626.85 to 627.85 m is missing. LST = lowstand systems tract; TST = transgressive systems tract; HST = highstand systems tract; MFS = maximum flooding surface. [a] Sequence stratigraphic framework of the studied NAS core from Lazar (2007). [b] TOC content calculated from U content (Liu et al., 2019).

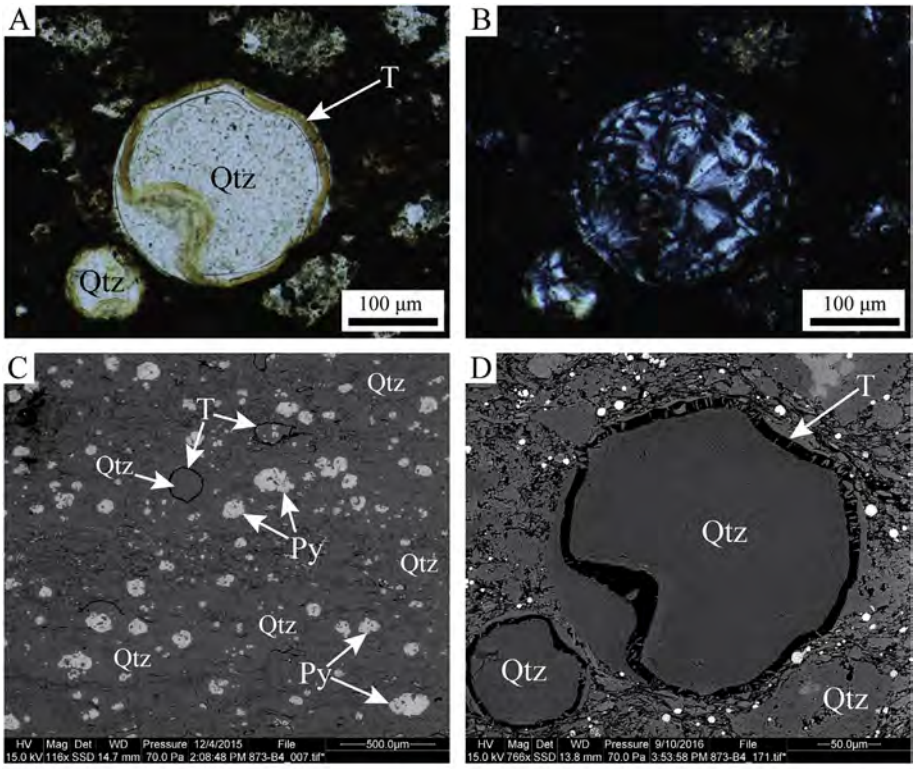

Fig. 5. Photomicrographs of shale samples near the MFS of sequence 4 at 613.85 m. This interval has 62.78% quartz, 56.68% bioquartz, 5.97% Al_2O_3 content, and a hardness value of 701. (A–B) Photomicrographs under an optical microscope. (C–F) SEM images (backscattered electron image). (A) Bioquartz precipitated in *Tasmanites* cysts, plane-polarized light. (B) Panel A under cross-polarized light. (C) SEM image of this interval mainly composed of authigenic quartz and pyrite. (D) SEM image of bioquartz precipitated in *Tasmanites* cysts in panel A. (E) Authigenic quartz and pyrite precipitated in *Tasmanites* cysts and microcrystalline quartz precipitated in the shale matrix. (F) Microcrystalline quartz precipitated in the shale matrix. T = *Tasmanites* cyst; Qtz = quartz; Py = pyrite.

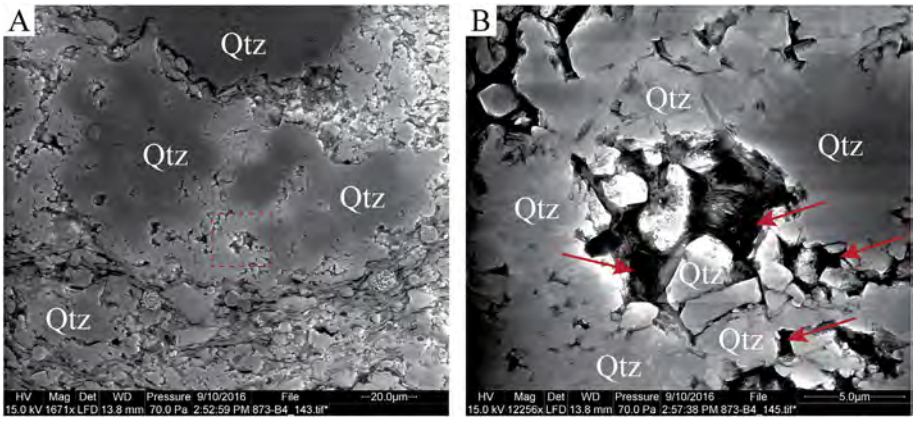

Fig. 6. SEM images (secondary electron image) of authigenic microcrystalline quartz network near the MFS of sequence 4 at 613.85 m. (A) Microcrystalline quartz in the matrix; (B) Close-up view of the red dashed framed area in panel A. Red arrows mark pores within microcrystalline quartz aggregates. Qtz = quartz. (For interpretation of the references to colour in this figure legend, the reader is referred to the Web version of this article.)

shale matrix (Fig. 5E − F). The size of microcrystalline quartz crystals ranges from < 1 to several μm (Fig. 6) and their occurrence in SEM images suggests that they are interconnected three-dimensionally (Figs. 5 and 6). Microcrystalline quartz in the matrix, together with the silica infill of *Tasmanites* cysts comprises an interconnected stiff network that enhances shale hardness (Liu and Schieber, 2017). Although authigenic quartz occludes some of the initial interparticle pore space, pores within this microcrystalline quartz fabric were protected from

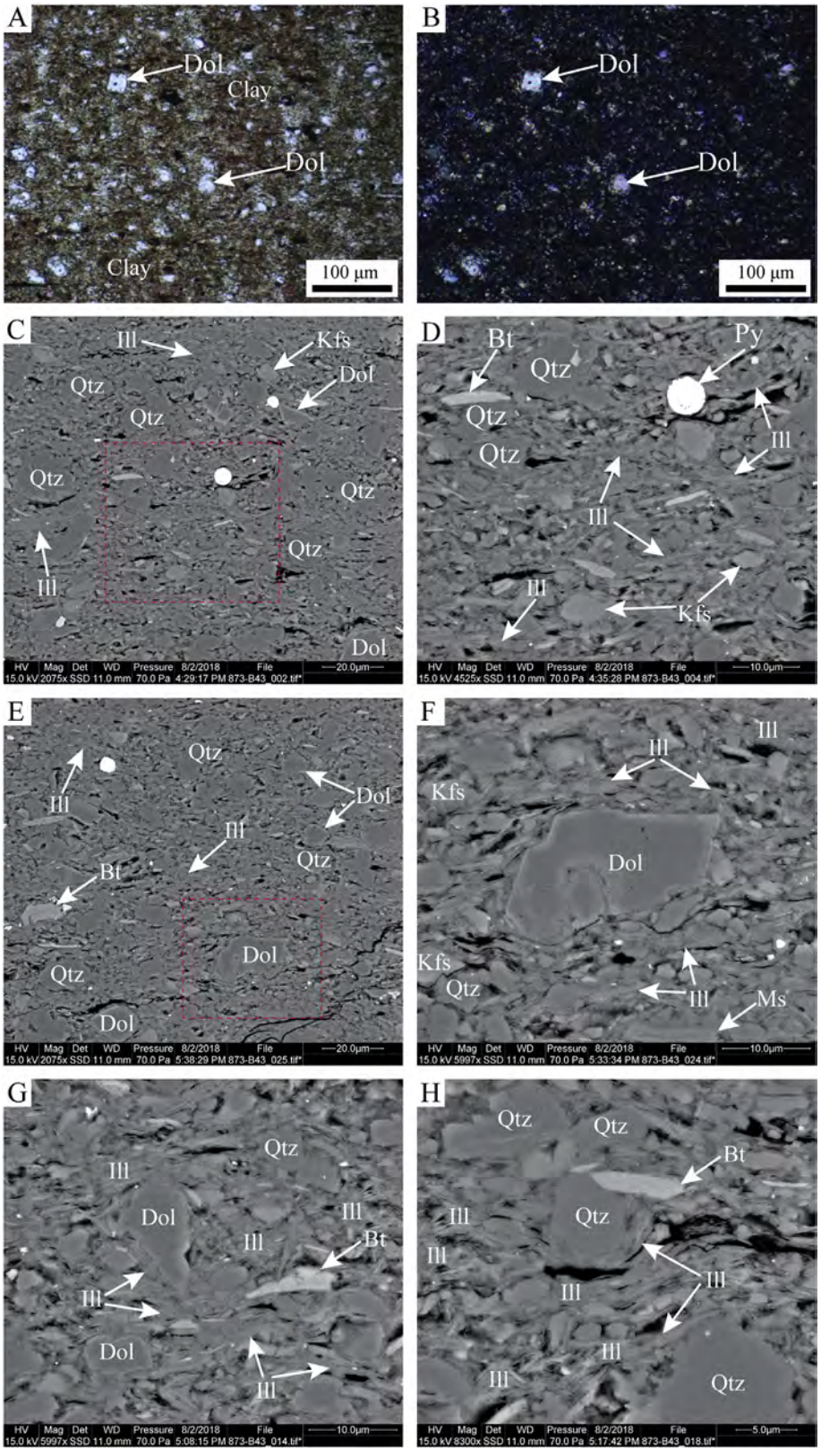

Fig. 7. Photomicrographs of shale samples in the HST of sequence 1 at 643.95 m. This interval has 24.55% quartz, 5.78% bioquartz, 18.38% Al_2O_3 content, and a hardness value of about 450. (A–B) Photomicrographs under an optical microscope. (C–H) SEM images (backscattered electron image). (A) Shales composed of clay minerals and dispersed silt-sized dolomite, plane-polarized light. (B) The same field of panel A under cross-polarized light. (C–H) SEM images of shales composed of clay minerals (mainly illite), pyrite, biotite, muscovite, and silt-sized quartz, dolomite, K-feldspar. Panel D and F are close-up views of the red dashed framed area in panel C and E, respectively. Note the differential compaction of clay minerals against rigid grains (quartz and dolomite) in panel G and H. Dol = dolomite; Qtz = quartz; Kfs = K-feldspar; Py = pyrite; Bt = biotite; Ms = muscovite; Ill = illite.

further compaction by the stiff quartz network (Fig. 6). Zhao et al. (2017) and Dong et al. (2019) also reported that the rigid bioquartz framework in black shales could preserve pore space between microcrystalline quartz crystals.

Hardness values are the lowest (average 450) in the upper part of the HST of sequence 1 (Fig. 4). The non-organic components of shales in this interval are mainly composed of clay minerals, pyrite, biotite, muscovite, and silt-sized detrital quartz, dolomite, and K-feldspar (Fig. 7). Clay minerals (mostly illite) dominate the mineralogical composition (Fig. 7). The differential compaction of clay minerals (Fig. 7G−H) against rigid grains (e.g., quartz and dolomite) demonstrates the ductile nature of the former. Clay mineral properties

dominate shale behavior (soft, ductile) because silt-size "hard" grains (detrital quartz, dolomite, and K-feldspar) are surrounded by clays and do not form a load-bearing fabric (Fig. 7).

5. Discussion

5.1. Control of rock composition on the hardness of black shales

The hardness of shales measured with the rebound method is considered a useful proxy for mechanical properties of tight shale reservoirs (Lee et al., 2014, 2016; Yang et al., 2015; Dong et al., 2017, 2018). For example, Lee et al. (2016) reported that the rebound hardness is positively correlated with uniaxial compressive strength in the Mississippian Barnett Shale of the Fort Worth Basin. Dong et al. (2017) reported that rebound hardness is positively correlated with log-derived brittleness in the Middle and Upper Devonian Horn River Group shale (Canada). High hardness typically indicates high brittleness of shales (Dong et al., 2017).

The mechanical strength of tight shale reservoirs is critically controlled by mineralogical composition (Aoudia et al., 2010; Sondergeld et al., 2010; Sone and Zoback, 2013a,b; Labani and Rezaee, 2015; Dong et al., 2017, 2018). Minerals in the NAS consist of quartz, clays (mostly illite), muscovite, K-feldspar, Na-feldspar, carbonates (dolomite and calcite), pyrite, marcasite, and minor amounts of heavy minerals (e.g., zircon, rutile; Frost and Shaffer, 1994). Quartz, calcite, and dolomite contents are commonly used as indicators of shale brittleness (Jarvie et al., 2007; Wang and Gale, 2009; Sondergeld et al., 2010; Jin et al., 2014; Hu et al., 2015; Xu and Sonnenberg, 2016; Zhang et al., 2017). In this study, we use the concentrations of Al_2O_3, CaO, and MgO as proxies for the contents of clay minerals, calcite, and dolomite, respectively (Ratcliffe et al., 2012a; Dong et al., 2017).

Quartz is commonly considered a brittle mineral, and its content is considered as one possible proxy for the brittleness of gas shales (Jarvie et al., 2007). In the NAS, hardness is positively correlated ($R^2 = 0.59$) with total quartz content (Fig. 8A), but shows an even better correlation ($R^2 = 0.71$) with bioquartz content (Fig. 8B). The reason why bioquartz rather than total quartz enhances hardness is that detrital quartz occurs as discrete particles within the shale matrix (Fig. 7), whereas bioquartz occurs as a pervasive cement and forms an interconnected stiff framework (Figs. 5 and 6). Similarly, Dong et al. (2017, 2018) reported that bioquartz can indicate the brittleness of Devonian black shales in Canada. Passey et al. (2010) suggested that bioquartz, not detrital quartz, is a favorable factor for successful reservoir stimulation in unconventional shale gas reservoirs. Walles (2004) reported that enrichment of diagenetic quartz cement is in many instances associated with shales that show natural fractures.

Bioquartz is a common constituent of the NAS (Fig. 4; Schieber, 1996; Schieber et al., 2000; Liu et al., 2019). The likely source of bioquartz in marine black shales is the dissolution of opaline skeletons of marine planktonic organisms such as radiolaria and sponges (Schieber, 1996; Schieber et al., 2000). Ti is generally associated with detrital heavy minerals such as rutile, and its content can be used as an indicator of terrestrial input (Brumsack, 2006). In cases where SiO_2/TiO_2 plots show a positive correlation a dominance of detrital quartz is indicated, whereas a negative correlation suggests the presence of biogenic input of silica (Peinerud et al., 2001; Nandy et al., 2014). Crossplots of Zr versus Si can also be used be used in an analogous fashion (Ratcliffe et al., 2012b; Socianu et al., 2015; Dong et al., 2017). In this study, the correlation between TiO_2 and SiO_2 content indicates a dominance of detrital quartz but with a significant proportion of bioquartz present, especially in samples from the Clegg Creek Member (Fig. 9), which is consistent with the bioquartz content calculated with Eq. (2).

In addition to biogenic quartz, microcrystalline quartz cement sourced from silica released during the smectite-to-illite transition can also increase the mechanical strength of shales (Peltonen et al., 2009; Thyberg et al., 2010; Thyberg and Jahren, 2011). However, the contribution of such a source is uncertain because the original smectite content at the time of deposition is not known. What is certain is that smectite (if any) has almost been completely transformed to illite or interstratified illite/smectite because no pure smectite was detected and only minor amounts of mixed-layer illite/smectite have been found in the NAS (Frost and Shaffer, 1994; Hover et al., 1996; Mastalerz et al., 2013). Hover et al. (1996) studied the fabrics, microtextures, and compositions of illite-rich samples from the NAS and suggested that the illite is authigenic. Generally, the smectite to illite conversion requires temperatures above 55 °C (Perry and Hower, 1970), yet the thermal maturity of the studied NAS core (0.55% R_o) suggests that it did not experience heating past 55 °C. However, this clay mineral transition also depends on time (Thyberg et al., 2010). Potter et al. (2005) suggested that mudstones older than Carboniferous have lost most of their smectite for that reason and are therefore dominated by illite and chlorite.

Carbonate minerals are generally considered to be a further shale component that enhances the brittleness of shales (Wang and Gale, 2009; Kumar et al., 2012; Jin et al., 2014; Hu et al., 2015; Dong et al., 2018). In this study, however, hardness does not correlate with CaO content ($R^2 = 0.04$) (Fig. 8C). A few Ca-rich samples at 648.39 and 637.66 m have also high hardness values (in excess of 600, higher than most samples), suggesting that calcite could potentially enhance the hardness of shales. However, these are rare isolated values (Fig. 4) that have not been recognized in other wells or in outcrop (Lazar, 2007) and likely represent localized concretionary growth. It is therefore highly unlikely that calcite plays a role in the broader context of stratigraphic variability of rock mechanical properties of the NAS.

Dolomite is also regarded as a brittleness enhancing mineral and its content has been used to calculate the brittleness index (BI) of other shale gas reservoirs (Wang and Gale, 2009). In this study, dolomite as represented by MgO shows no correlation to hardness ($R^2 = 0.02$) (Fig. 8D) likely because dolomite occurs as isolated grains within the shale matrix (Figs. 7 and 10). Dispersed "hard" grains (e.g., detrital quartz and dolomite) generally do not increase the brittleness of shales (Milliken and Olson, 2017).

X-ray diffraction analysis of the NAS samples shows that its clay component is dominated by illite, and contains minor amounts of kaolinite and chlorite (Frost and Shaffer, 1994; Mastalerz et al., 2013, 2016). Clay minerals are generally thought of as ductile, prone to reduce the brittleness of shales (Jarvie et al., 2007; Wang and Gale, 2009; Aoudia et al., 2010; Passey et al., 2010; Kumar et al., 2012; Zargari et al., 2013; Labani and Rezaee, 2015; Dong et al., 2017, 2018). Hardness is negatively correlated with Al_2O_3 content ($R^2 = 0.64$) (Fig. 8E), which together with the differential compaction of clay minerals against rigid grains (e.g., quartz, dolomite, and pyrite; Fig. 7G − H), suggests that clay minerals are indeed ductile components in the NAS. Dong et al. (2017, 2018) also reported that hardness is strongly negatively correlated with Al_2O_3 content in Devonian black shales in Canada. Fishman et al. (2012) suggested that the Upper Jurassic Kimmeridge Clay Formation underwent intense compaction because of high contents of ductile clay minerals, and that this caused the collapse of pores that had formed in organic matter in the course of oil and gas generation.

Organic matter has a lower density and mechanical strength compared to minerals and is considered a ductile component in organic-rich shales (Walles, 2004; Aoudia et al., 2010; Kumar et al., 2012; Zargari et al., 2013; Eliyahu et al., 2015; Labani and Rezaee, 2015; Li et al., 2018a,b), although thermal maturity and organic matter type can to some degree affect the elastic properties of organic matter (Mba and Prasad, 2010; Emmanuel et al., 2016; Yang et al., 2017). The Young's modulus of organic matter in black shales ranges from 0 to 25 GPa (Eliyahu et al., 2015), which is much lower than that of quartz (77–96 GPa; Mavko et al., 2009), calcite (74–83 GPa; Mavko et al., 2009), and clay minerals (21–55 GPa; Eliyahu et al., 2015, and

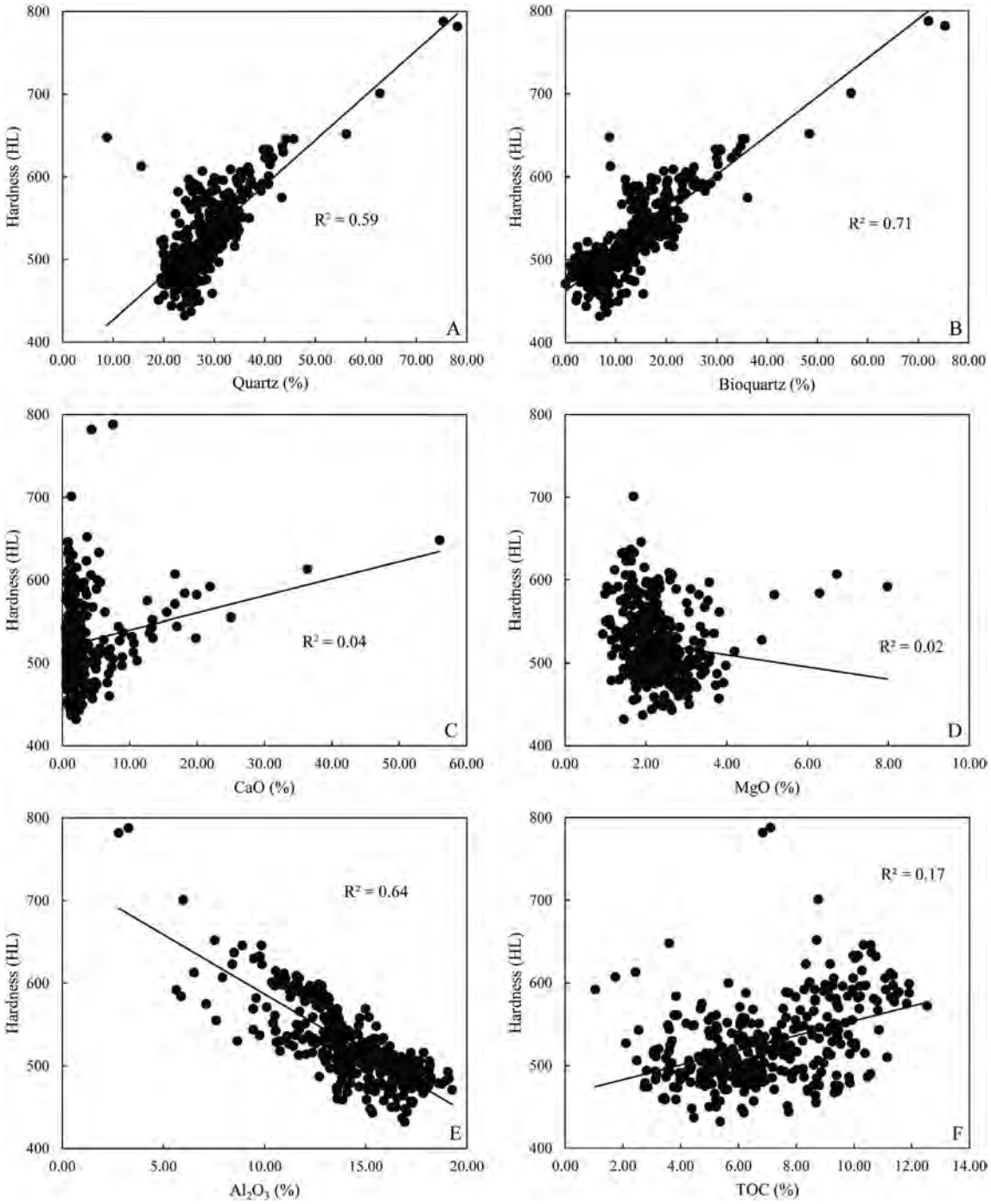

Fig. 8. Correlations between hardness and total quartz, bioquartz, CaO, MgO, Al_2O_3, and TOC content for the studied NAS core.

references therein). In this study, however, a weak positive correlation exists between hardness and TOC content (Fig. 8F) because the stratigraphic distribution of TOC content is very similar to the bioquartz content profile (Fig. 4; Liu et al., 2019), and the influence of organic matter on the hardness of shales is counteracted by bioquartz. Likewise, Dong et al. (2017) reported that no negative relationship exists between hardness and TOC content in the Horn River Group shale (Canada).

Pyrite nodules in the NAS have an average hardness value of about 750, which is higher than the hardness of localized calcite cementation (hardness 648) at 648.39 m, but slightly lower than that of the highly bioquartz enriched interval (hardness 782) at 614.38 m (Fig. 4). The Young's modulus of pyrite has been reported to be higher than that of quartz (Mavko et al., 2009). However, because pyrite occurs as isolated grains (framboids, small concretions) it has minimal influence on the hardness of the NAS.

Mineral-composition-based brittleness indices are commonly used to evaluate the fracturability of tight shale reservoirs (Table 1; Jarvie et al., 2007; Wang and Gale, 2009; Sondergeld et al., 2010; Jin et al., 2014; Hu et al., 2015; Xu and Sonnenberg, 2016; Zhang et al., 2017). However, some of these indices (Table 1) do not include the fraction of organic matter (Jarvie et al., 2007; Sondergeld et al., 2010; Jin et al., 2014) and may result in inappropriate brittleness assessments because of the low strength and ductile character of organic matter (Eliyahu et al., 2015; Labani and Rezaee, 2015). In this study, we propose a new BI on the basis of rock composition to characterize the brittleness of black shales. The new BI is defined as the content of bioquartz in bulk

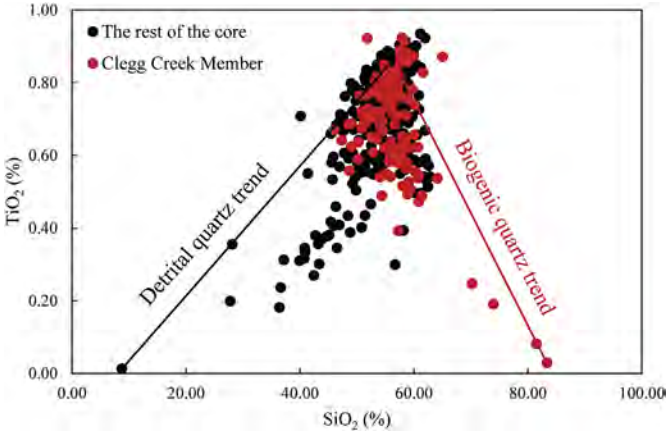

Fig. 9. Cross-plot between TiO_2 and SiO_2 content in the studied NAS core. Note that the detrital quartz trend indicates a dominance of detrital quartz, not that all quartz are detrital. The same is true for the biogenic quartz trend, which suggests a common presence of bioquartz, not that all quartz is biogenic.

Table 1
Brittleness index (BI) of shales based on mineralogical composition from the literature and this study.

Formula	Source
$BI = \frac{W_{quartz}}{W_{(quartz+carbonate+clay)}} \times 100\%$	Jarvie et al., 2007; Sondergeld et al. (2010)
$BI = \frac{W_{(quartz+dolomite)}}{W_{(quartz+dolomite+limestone+clay+TOC)}} \times 100\%$	Wang and Gale (2009)
$BI = \frac{W_{(quartz+feldspar+mica+carbonate)}}{W_{total\ mineral}} \times 100\%$	Jin et al. (2014)
$BI = \frac{W_{(quartz+dolomite+calcite)}}{W_{(quartz+dolomite+calcite+clay+TOC)}} \times 100\%$	Hu et al. (2015)
$BI = \frac{W_{(quartz+calcite+dolomite+feldspar+pyrite)}}{W_{(quartz+calcite+dolomite+feldspar+pyrite+clay+TOC)}} \times 100\%$	Xu and Sonnenberg (2016)
$BI = \frac{W_{(quartz+dolomite+pyrite)}}{W_{total}} \times 100\%$	Zhang et al. (2017)
$BI = \frac{W_{bioquartz}}{W_{total}} \times 100\%$	This study

W_{total} = total weight percent of samples (100%); W_X = weight percent of mineral X in samples; TOC = total organic carbon; bioquartz = biogenic quartz.

shales (Table 1), reflecting the degree of matrix cementation and interconnectedness of bioquartz in the matrix (Figs. 5 and 6). Bohacs et al. (2013) also suggested that biogenic quartz provides strength (brittleness) to tight mudstone reservoirs. Because dolomite mainly occurs as isolated grains in the NAS (Fig. 10), it is not considered to generate brittle behavior (Milliken and Olson, 2017). When dolomite or calcite cement is abundant enough to become fabric supporting, we recommend adding dolomite or calcite content to BI calculations as suggested by other studies (Wang and Gale, 2009; Sondergeld et al., 2010; Jin et al., 2014; Hu et al., 2015; Xu and Sonnenberg, 2016; Zhang et al., 2017). It should be noted that if multiple minerals are included in BI calculations, minerals should be weighted according to their overall contribution to the mechanical strength of bulk shales (Mathia et al., 2016).

The studied NAS core is in early oil window according to the thermal maturity (0.55% R_o). The NAS within the main oil and gas windows is expected to have higher hardness because of enhanced mechanical compaction and cementation, increased stiffness of organic matter, and redistribution of solid bitumen (Mondol et al., 2007; Mba and Prasad, 2010; Thyberg et al., 2010; Thyberg and Jahren, 2011; Zargari et al., 2013; Emmanuel et al., 2016; Dong et al., 2018). However, because these factors affect the NAS as a whole, the stratigraphic distribution pattern of hardness should remain the same.

5.2. Mechanical stratigraphy

The term "mechanical stratigraphy" refers to variations of rock mechanical properties associated with stratigraphic units within a given formation (Corbett et al., 1987; Gross, 2003; Laubach et al., 2009; Miskimins, 2012) and is especially useful in evaluating unconventional shale reservoirs because it can be used to target potentially productive

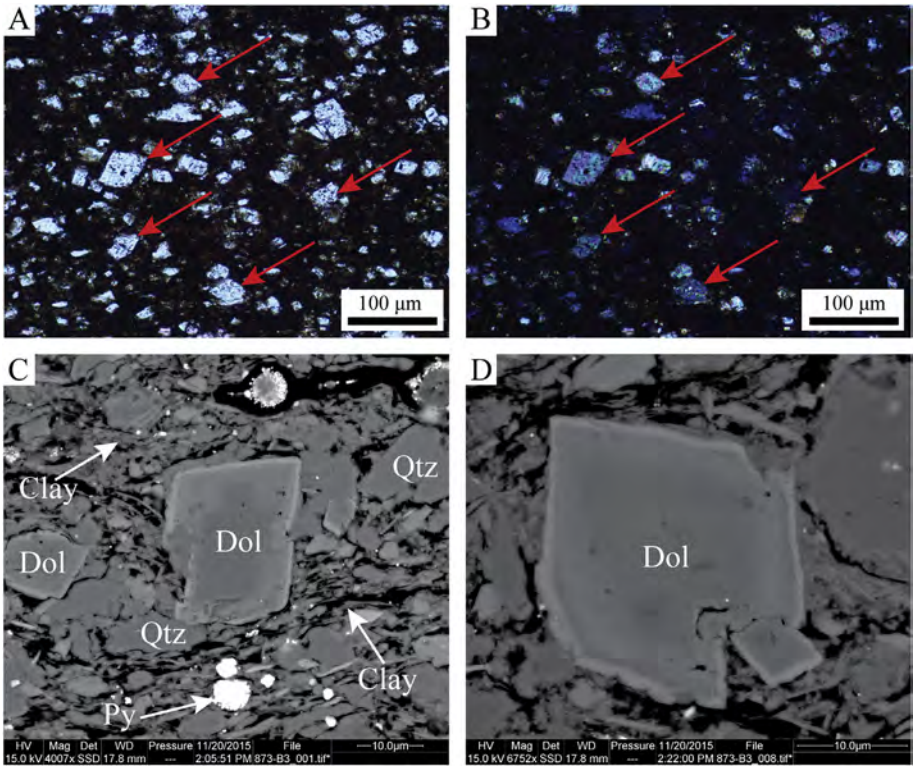

Fig. 10. Photomicrographs of dolomite in the NAS. (A) Dolomite grains (red arrows) in clay matrix, plane-polarized light; (B) The same field of panel A under cross-polarized light; (C–D) SEM images (backscattered electron image) of dolomite grains in clay matrix. Dol = dolomite; Qtz = quartz; Py = pyrite. (For interpretation of the references to colour in this figure legend, the reader is referred to the Web version of this article.)

intervals (Miskimins, 2012). Previous studies have reported stratigraphic variations of mechanical properties within black shale successions (Harris et al., 2011; Lash and Blood, 2011; Slatt and Abousleiman, 2011; Liu et al., 2018). For example, Harris et al. (2011) reported stratigraphic variations of Young's modulus and Poisson's ratio in the Woodford Shale of the Permian Basin that were interpreted to reflect sea-level fluctuations at the time of deposition. In the studied NAS core, hardness increases in TSTs until reaching MFSs, and subsequently decreases in HSTs towards sequence boundaries except in the Blocher Member (Fig. 4). Similarly, Dong et al. (2018) reported increases in Young's modulus, brittleness, and hardness towards the MFS within a depositional sequence in the Upper Devonian Duvernay Formation (Canada) because of reduced clay input and increased bioquartz content in TSTs. Lash and Blood (2011) suggested that an increase in diagenetic silica and reduction of clay mineral abundances upward through the TST could enhance the brittleness of the Devonian gas shales of the Appalachian Basin. In the NAS, the increase of bioquartz content in TSTs and decrease in HSTs likely resulted from the variation of clastic supply controlled by relative sea-level fluctuations (Liu et al., 2019).

In most of the 1-3 Kavanaugh core, the stratigraphic variability of hardness is controlled by the distribution of bioquartz (Figs. 4 and 8). The stratigraphic distribution of hardness in the Blocher Member, however, differs from other members (Fig. 4). Unlike in other members, in the Blocher Member, hardness shows an initial short increase and subsequent decrease (Fig. 4). A potential explanation is that when sea level began to rise during deposition of the Blocher Member, siliciclastic detritus was in limited supply, and carbonate detritus eroded from laterally exposed carbonate rocks was deposited in the Illinois basin (Schieber and Lazar, 2004; Lazar, 2007). As a result, there was not much clay to impart ductile behavior, and carbonates could via overgrowth and recrystallization strengthen the rock, and add to the hardness provided by the bioquartz component. As relative sea level dropped, more clastic materials were transported to the basin. Therefore, the upper half of the Blocher Member (HST) is characterized by high clay minerals content and behaves as expected for HSTs in the NAS (Fig. 4).

The Clegg Creek Member shows the highest hardness (average 565) in the NAS because of strong enrichment of bioquartz (average 20.38%). Because it is also the most organic-rich section in the NAS (Lazar, 2007; Liu et al., 2019), it represents an optimal interval for hydraulic stimulation in areas with appropriate thermal maturity. The MFS intervals in other members, except the Blocher Member, could also be potential fracturing zones. However, other screening parameters such as porosity, permeability, oil saturation, gas content, thermal maturity, reservoir pressure, and structural complication should also be considered when targeting a potentially productive zone (Wang and Gale, 2009; Passey et al., 2010; Sondergeld et al., 2010; Slatt, 2011; Jarvie, 2012a,b; Bohacs et al., 2013).

6. Conclusions

High-resolution rebound hardness tests and geochemical measurements on a NAS core allowed us to examine the stratigraphic variability of rock mechanical properties of the NAS and the influence of rock composition on the hardness of black shales. Specific conclusions are as follows:

(1) Total quartz and bioquartz content in the NAS averages 27.64% and 12.88%, respectively. Approximately 47% of the total quartz appears to be of biogenic origin. Bioquartz occurs as authigenic quartz precipitated in *Tasmanites* cysts, and as microcrystalline quartz in the shale matrix.
(2) Bioquartz content critically controls the hardness of the NAS because it forms an interconnected stiff framework. Dispersed “hard” grains (e.g., detrital quartz, feldspar, and dolomite) surrounded by ductile clay minerals do not generate brittle behavior. Clay minerals reduce the hardness of shales. Organic matter, although considered a ductile component, shows a weak positive correlation with hardness, mainly because organic matter content has a similar stratigraphic distribution pattern as bioquartz content.
(3) A mineral-composition-based brittleness index was proposed for the NAS on the basis of bioquartz abundance. This index could also be adapted to characterize the rock mechanical properties of other tight shale reservoirs.
(4) A stratigraphic distribution pattern of rock mechanical properties exists within the NAS that reflects the underlying sequence stratigraphic framework. Hardness increases in TSTs, reaches a maximum at MFSs, and decreases in HSTs except for the Blocher Member.

Acknowledgments

This research was supported by the sponsors of the Indiana University Shale Research Consortium (Anadarko, Chevron, ConocoPhillips, ExxonMobil, Shell, Statoil, Marathon, Whiting, Wintershall, and PetroChina (Project number 2016B-0302-01)) and an American Association of Petroleum Geologists Foundation Grants-in-Aid Award. An NSF equipment grant to Juergen Schieber (EAR-0318769) provided funds for the purchase of the analytical SEM that was used for acquiring the images used in this study. Mastalerz's contribution is based upon work supported by the U.S. Department of Energy, Office of Science, Office of Basic Energy Sciences, Chemical Sciences, Geosciences, and Biosciences Division under Award Number DE-SC0006978. Financial support for Bei Liu from the China Scholarship Council is also gratefully acknowledged.

References

Aoudia, K., Miskimins, J.L., Harris, N.B., Mnich, C.A., 2010. Statistical analysis of the effects of mineralogy on rock mechanical properties of the Woodford shale and the associated impacts for hydraulic fracture treatment design. In: 44th US Rock Mechanics Symposium and 5th US-Canada Rock Mechanics Symposium. American Rock Mechanics Association, Salt Lake City, Utah, USA, June 27–30, 2010, 11 p.

Beier, J.A., Hayes, J.M., 1989. Geochemical and isotopic evidence for paleoredox conditions during deposition of the Devonian-Mississippian New Albany Shale, southern Indiana. Geol. Soc. Am. Bull. 101, 774–782.

Bohacs, K.M., Passey, Q.R., Rudnicki, M., Esch, W.L., Lazar, O.R., 2013. The spectrum of fine-grained reservoirs from 'shale gas' to 'shale oil'/tight liquids: essential attributes, key controls, practical characterization. In: International Petroleum Technology Conference. Beijing, China, March 26–28, 2013, Paper IPTC 16676, 16 p.

Brumsack, H.J., 2006. The trace metal content of recent organic carbon-rich sediments: implications for Cretaceous black shale formation. Palaeogeogr. Palaeoclimatol. Palaeoecol. 232, 344–361.

Buschbach, T.C., Kolata, D.R., 1990. Regional setting of Illinois basin. In: In: Leighton, M.W., Kolata, D.R., Oltz, D.F., Eidel, J.J. (Eds.), Interior Cratonic Basins, vol. 51. AAPG Memoir, pp. 29–55.

Bustin, A.M., Bustin, R.M., 2012. Importance of rock properties on the producibility of gas shales. Int. J. Coal Geol. 103, 132–147.

Campbell, G., 1946. New Albany shale. GSA Bull. 57, 829–908.

Chou, M.-I.M., Dickerson, D.R., Chou, S.-F.J., Sargent, M.L., 1991. Hydrocarbon Source Potential and Organic Geochemical Nature of Source Rocks and Crude Oils in the Illinois Basin, vol. 136. Illinois State Geological Survey, Illinois Petroleum, Illinois, pp. 39.

Corbett, K., Friedman, M., Spang, J., 1987. Fracture development and mechanical stratigraphy of Austin Chalk, Texas. AAPG Bull. 71, 17–28.

Dong, T., Harris, N.B., Ayranci, K., Yang, S., 2017. The impact of rock composition on geomechanical properties of a shale formation: Middle and Upper Devonian Horn River Group shale, Northeast British Columbia, Canada. AAPG Bull. 101, 177–204.

Dong, T., Harris, N.B., Knapp, L.J., McMillan, J.M., Bish, D.L., 2018. The effect of thermal maturity on geomechanical properties in shale reservoirs: an example from the Upper Devonian Duvernay Formation, Western Canada Sedimentary Basin. Mar. Pet. Geol. 97, 137–153.

Dong, T., He, S., Chen, M., Hou, Y., Guo, X., Wei, C., Han, Y., Yang, R., 2019. Quartz types and origins in the paleozoic Wufeng-Longmaxi Formations, Eastern Sichuan Basin, China: implications for porosity preservation in shale reservoirs. Mar. Pet. Geol. 106, 62–73.

Eliyahu, M., Emmanuel, S., Day-Stirrat, R.J., Macaulay, C.I., 2015. Mechanical properties of organic matter in shales mapped at the nanometer scale. Mar. Pet. Geol. 59, 294–304.

Emmanuel, S., Eliyahu, M., Day-Stirrat, R.J., Hofmann, R., Macaulay, C.I., 2016. Impact

of thermal maturation on nano-scale elastic properties of organic matter in shales. Mar. Pet. Geol. 70, 175–184.
Fishman, N.S., Hackley, P.C., Lowers, H.A., Hill, R.J., Egenhoff, S.O., Eberl, D.D., Blum, A.E., 2012. The nature of porosity in organic-rich mudstones of the upper Jurassic Kimmeridge Clay Formation, north sea, offshore United Kingdom. Int. J. Coal Geol. 103, 32–50.
Frost, J.K., Shaffer, N.R., 1994. Mineralogy and geochemistry. In: In: Hasenmueller, N.R., Comer, J.B. (Eds.), Gas Potential of the New Albany Shale (Devonian and Mississippian) in the Illinois Basin, vol. 2. Gas Research Institute, GRI-00/0068, Illinois Basin Studies, pp. 41–45.
Gale, J.F., Laubach, S.E., Olson, J.E., Eichhubl, P., Fall, A., 2014. Natural fractures in shale: a review and new observations. AAPG Bull. 98, 2165–2216.
Gale, J.F., Reed, R.M., Holder, J., 2007. Natural fractures in the Barnett Shale and their importance for hydraulic fracture treatments. AAPG Bull. 91, 603–622.
Ghanizadeh, A., Clarkson, C.R., Aquino, S., Ardakani, O.H., Sanei, H., 2015. Petrophysical and geomechanical characteristics of Canadian tight oil and liquid-rich gas reservoirs: II. Geomechanical property estimation. Fuel 153, 682–691.
Grieser, B., Bray, J.M., 2007. Identification of production potential in unconventional reservoirs. In: Production and Operations Symposium. Society of Petroleum Engineers, Oklahoma City, Oklahoma, USA, March 31 – April 3, 2007, SPE Paper 106623, 6 p.
Gross, M.R., 2003. Mechanical stratigraphy: the brittle perspective. GSA Abstr. Progr. 35, 641.
Hamilton-Smith, T., Hasenmueller, N.R., Boberg, W.S., Smidchens, Z., Frankie, W.T., 1994. Gas production. In: In: Hasenmueller, N.R., Comer, J.B. (Eds.), Gas Potential of the New Albany Shale (Devonian and Mississippian) in the Illinois Basin, vol. 2. Gas Research Institute, GRI-92/0391, Illinois Basin Studies, pp. 23–40.
Harris, N.B., Miskimins, J.L., Mnich, C.A., 2011. Mechanical anisotropy in the Woodford shale, Permian Basin: origin, magnitude, and scale. Lead. Edge 30, 284–291.
Heidlauf, D.T., Hsui, A.T., Klein, G.D., 1986. Tectonic subsidence analysis of the Illinois Basin. J. Geol. 94, 779–794.
Hill, D.G., Nelson, C.R., 2000. Gas productive fractured shales: an overview and update. Gastips 6, 4–13.
Hover, V.C., Peacor, D.R., Walter, L.M., 1996. STEM/AEM evidence for preservation of burial diagenetic fabrics in Devonian shales: Implications for fluid/rock interaction in cratonic basins (U.S.A.). J. Sediment. Res. 66, 519–530.
Hu, Y., Gonzalez Perdomo, M.E., Wu, K., Chen, Z., Zhang, K., Yi, J., Ren, G., Yu, Y., 2015. New models of brittleness index for shale gas reservoirs: weights of brittle minerals and rock mechanics parameters. In: SPE Asia Pacific Unconventional Resources Conference and Exhibition. Society of Petroleum Engineers, Brisbane, Australia, November 9–11, 2015, SPE Paper 177010, 13 p.
Jarvie, D.M., 2012a. Shale resource systems for oil and gas: Part 1—Shale-gas resource systems. In: In: Breyer, J.A. (Ed.), Shale Reservoirs— Giant Resources for the 21st Century, vol. 97. AAPG Memoir, pp. 69–87.
Jarvie, D.M., 2012b. Shale resource systems for oil and gas: Part 1—Shale-oil resource systems. In: In: Breyer, J.A. (Ed.), Shale Reservoirs— Giant Resources for the 21st Century, vol. 97. AAPG Memoir, pp. 89–119.
Jarvie, D.M., Hill, R.J., Ruble, T.E., Pollastro, R.M., 2007. Unconventional shale-gas systems: The Mississippian Barnett Shale of north-central Texas as one model for thermogenic shale-gas assessment. AAPG Bull. 91 (4), 475–499.
Jin, X., Shah, S.N., Roegiers, J.C., Zhang, B., 2014. Fracability evaluation in shale reservoirs-an integrated petrophysics and geomechanics approach. In: SPE Hydraulic Fracturing Technology Conference. Society of Petroleum Engineers, the Woodlands, Texas, USA, February 4–6, 2014, SPE Paper 168589, 14 p.
Kumar, V., Sondergeld, C.H., Rai, C.S., 2012. Nano to macro mechanical characterization of shale. In: SPE Annual Technical Conference and Exhibition. Society of Petroleum Engineers, San Antonio, Texas, USA, October 8–10, 2012, SPE Paper 159804, 23 p.
Labani, M.M., Rezaee, R., 2015. The importance of geochemical parameters and shale composition on rock mechanical properties of gas shale reservoirs: A case study from the Kockatea Shale and Caryngnia Formation from the Perth Basin, Western Australia. Rock Mech. Rock Eng. 48, 1249–1257.
Lash, G., Blood, R., 2011. Sequence Stratigraphy as Expressed by Shale Source Rock and Reservoir Characteristics—Examples from the Devonian Succession, Appalachian Basin. AAPG Search and Discovery, 80168.
Laubach, S.E., Olson, J.E., Gross, M.R., 2009. Mechanical and fracture stratigraphy. AAPG Bull. 93, 1413–1426.
Lazar, O.R., 2007. Redefinition of the New Albany Shale of the Illinois Basin: an Integrated, Stratigraphic, Sedimentologic, and Geochemical Study (Ph.D. dissertation). Indiana University, Bloomington 336 p.
Lee, J.S., Kieschnick, J., Geyer, C., Brumley, J., DeSpain, L., 2016. Comparison of Different Methods to Estimate Uniaxial Compressive Strength in a Barnett Shale. In: 50th US Rock Mechanics/Geomechanics Symposium. American Rock Mechanics Association, Houston, Texas, USA, June 26 – 29, 2016, 9 p.
Lee, J.S., Smallwood, L., Morgan, E., 2014. New application of rebound hardness numbers to generate logging of unconfined compressive strength in laminated shale formations. In: 48th US Rock Mechanics/Geomechanics Symposium. American Rock Mechanics Association, Minneapolis, Minnesota, USA, June 1 – 4, 2014, 7 p.
Li, C., Ostadhassan, M., Abarghani, A., Fogden, A., Kong, L., 2018a. Multi-scale evaluation of mechanical properties of the Bakken shale. J. Mater. Sci. 1 – 19.
Li, C., Ostadhassan, M., Guo, S., Gentzis, T., Kong, L., 2018b. Application of PeakForce tapping mode of atomic force microscope to characterize nanomechanical properties of organic matter of the Bakken Shale. Fuel 233, 894–910.
Lineback, J.A., 1964. Stratigraphy and Depositional Environment of the New Albany Shale (Upper Devonian and Lower Mississippian) in Indiana (Ph.D. dissertation). Indiana University 136 p.
Lineback, J.A., 1968. Subdivisions and depositional environments of New Albany Shale (Devonian-Mississippian) in Indiana. AAPG Bull. 52, 1291–1303.
Liu, B., Schieber, J., 2017. Authigenic minerals formation and detrital minerals accumulation associated with Tasmanites cysts, and initial depositional porosity in the New Albany Shale, Illinois Basin. In: AAPG Annual Convention and Exhibition, Houston, TX, USA, April 2 – 5, 2017.
Liu, B., Schieber, J., Mastalerz, M., Lazar, R., Teng, J., 2018. Rock mechanical properties variation in the sequence stratigraphic context of the Upper Devonian New Albany Shale, Illinois Basin. In: GSA Annual Meeting, Indianapolis, IN, USA, November 4 – 7, 2018, https://doi.org/10.1130/abs/2018AM-318079.
Liu, B., Schieber, J., Mastalerz, M., Teng, J., 2019. Organic matter content and type variation in the sequence stratigraphic context of the Upper Devonian New Albany Shale, Illinois Basin. Sediment. Geol. 383, 101–120.
Martini, A.M., Walter, L.M., McIntosh, J.C., 2008. Identification of microbial and thermogenic gas components from Upper Devonian black shale cores, Illinois and Michigan basins. AAPG Bull. 92, 327–339.
Mastalerz, M., Karayigit, A., Hampton, L., Drobniak, A., 2016. Variations in gas content in organic matter-rich low maturity shale: Example from the New Albany Shale in the Illinois Basin. Jacobs J. Pet. Nat. Gas 1, 005.
Mastalerz, M., Schimmelmann, A., Drobniak, A., Chen, Y., 2013. Porosity of Devonian and Mississippian New Albany Shale across a maturation gradient: Insights from organic petrology, gas adsorption, and mercury intrusion. AAPG Bull. 97, 1621–1643.
Mathia, E., Ratcliffe, K., Wright, M., 2016. Brittleness Index-A Parameter to Embrace or Avoid? In: Unconventional Resources Technology Conference. SPE-AAPG-SEG, San Antonio, Texas, USA, August 1 – 3, 2016, Paper 2448745, 10 p.
Mavko, G., Mukerji, T., Dvorkin, J., 2009. The Rock Physics Handbook: Tools for Seismic Analysis of Porous Media. Cambridge University Press, Cambridge 511 p.
Mba, K., Prasad, M., 2010. Mineralogy and its contribution to anisotropy and kerogen stiffness variations with maturity in the Bakken shales. In: SEG Annual Meeting, Denver, Colorado, USA, October 17 – 22, 2010. SEG Technical Program Expanded Abstracts, pp. 2612–2616.
McFarlan, A.C., 1943. The Geology of Kentucky. University of Kentucky, Lexington 531 p.
McLaughlin, P.I., Emsbo, P., Desrochers, A., Bancroft, A., Brett, C.E., Riva, J.F., Premo, W., Neymark, L., Achab, A., Asselin, E., Emmons, M.M., 2016. Refining 2 km of Ordovician chronostratigraphy beneath Anticosti Island utilizing integrated chemostratigraphy. Can. J. Earth Sci. 53, 865–874.
Milliken, K.L., Olson, T., 2017. Silica diagenesis, porosity evolution, and mechanical behavior in siliceous mudstones, Mowry Shale (Cretaceous), Rocky Mountains, U.S.A. J. Sediment. Res. 87, 366–387.
Miskimins, J.L., 2012. The Impact of Mechanical Stratigraphy on Hydraulic Fracture Growth and Design Considerations for Horizontal Wells. AAPG Search and Discovery (Article No. 41102).
Mondol, N.H., Bjørlykke, K., Jahren, J., Høeg, K., 2007. Experimental mechanical compaction of clay mineral aggregates—Changes in physical properties of mudstones during burial. Mar. Pet. Geol. 24, 289–311.
Nandy, D., Sonnenberg, S., Humphrey, J.D., 2014. Application of inorganic geochemical studies for characterization of Bakken Shales, Williston Basin, North Dakota and Montana. In: Unconventional Resources Technology Conference. SPE-AAPG-SEG, Denver, Colorado, USA, August 25 – 27, 2014, Paper 1922974, 11 p.
Nuttall, B.C., Parris, T.M., Beck, G., Willette, D.C., Mastalerz, M., Crockett, J., 2015. Oil Production from Low-Maturity Organic-Rich Shale: an Example from the Devonian New Albany Shale in the Illinois Basin, Breckinridge County, Kentucky. AAPG Search and Discovery (Article No. 51196).
Passey, Q.R., Bohacs, K.M., Esch, W.L., Klimentidis, R., Sinha, S., 2010. From oil-prone source rock to gas-producing shale reservoir-geologic and petrophysical characterization of unconventional shale-gas reservoirs. In: Chinese Petroleum Society/Society of Petroleum Engineers International Oil and Gas Conference and Exhibition, Beijing, China, June 8 – 10, 2010, SPE Paper 131350, 29 p.
Peinerud, E.K., Ingri, J., Pontér, C., 2001. Non-detrital Si concentrations as an estimate of diatom concentrations in lake sediments and suspended material. Chem. Geol. 177, 229–239.
Peltonen, C., Marcussen, Ø., Bjørlykke, K., Jahren, J., 2009. Clay mineral diagenesis and quartz cementation in mudstones: The effects of smectite to illite reaction on rock properties. Mar. Pet. Geol. 26, 887–898.
Perry, E., Hower, J., 1970. Burial diagenesis in Gulf Coast pelitic sediments. Clay Clay Miner. 18, 165–177.
Potter, P.E., Maynard, J.B., Depetris, P.J., 2005. Mud and Mudstones: Introduction and Overview. Springer-Verlag, Berlin, pp. 127–155.
Ratcliffe, K.T., Wright, A.M., Schmidt, K., 2012a. Application of inorganic whole-rock geochemistry to shale resource plays: an example from the Eagle Ford Shale Formation, Texas. Sediment. Rec. 10, 4–9.
Ratcliffe, K., Wright, M., Spain, D., 2012b. Unconventional methods for unconventional plays: Using elemental data to understand shale resource plays. PESA News Resour. 89–93.
Rickman, R., Mullen, M.J., Petre, J.E., Grieser, W.V., Kundert, D., 2008. A practical use of shale petrophysics for stimulation design optimization: All shale plays are not clones of the Barnett Shale. In: SPE Annual Technical Conference and Exhibition. Society of Petroleum Engineers, Denver, Colorado, USA, September 21–24, 2008, SPE Paper 115258, 11 p.
Ritz, E., Honarpour, M., Dula, W.F., Dvorkin, J.P., 2014. Core hardness testing and data integration for unconventionals. In: Unconventional Resources Technology Conference. SPE-AAPG-SEG, Denver, Colorado, USA, August 25 – 27, 2014, Paper 1916004, 12 p.
Ross, D.J.K., Bustin, R.M., 2009. Investigating the use of sedimentary geochemical proxies for paleoenvironment interpretation of thermally mature organic-rich strata: examples from the Devonian–Mississippian shales, Western Canadian Sedimentary Basin. Chem. Geol. 260, 1–19.

Rowe, H., Hughes, N., Robinson, K., 2012. The quantification and application of handheld energy-dispersive x-ray fluorescence (ED-XRF) in mudrock chemostratigraphy and geochemistry. Chem. Geol. 324, 122–131.
Schieber, J., 1996. Early diagenetic silica deposition in algal cysts and spores: A source of sand in black shales? J. Sediment. Res. 66, 175–183.
Schieber, J., 1998. Developing a sequence stratigraphic framework for the Late Devonian Chattanooga Shale of the southeastern USA: Relevance for the Bakken Shale. In: In: Christopher, J.E., Gilboy, C.F., Paterson, D.F., Bend, S.L. (Eds.), Eighth International Williston Basin Symposium, vol. 13. Saskatchewan Geological Society Special Publication, pp. 58–68.
Schieber, J., Krinsley, D., Riciputi, L., 2000. Diagenetic origin of quartz silt in mudstones and implications for silica cycling. Nature 406, 981–985.
Schieber, J., Lazar, R.O., 2004. Devonian Black Shales of the Eastern U.S.: New Insights into Sedimentology and Stratigraphy from the Subsurface and Outcrops in the Illinois and Appalachian Basins. Indiana Geol. Surv Open File Study 04–05, 90 p.
Slatt, R., 2011. Important geological properties of unconventional resource shales. Cent. Eur. J. Geosci. 3, 435–448.
Slatt, R.M., Abousleiman, Y., 2011. Merging sequence stratigraphy and geomechanics for unconventional gas shales. Lead. Edge 30, 274–282.
Socianu, A., Kaszuba, J., Gustason, G., 2015. Importance of core and outcrop investigations for evaluating TOC distribution in unconventional systems: an example from the Mowry Shale. In: Unconventional Resources Technology Conference. SPE-AAPG-SEG, San Antonio, Texas, July 20 – 22, 2015, Paper 2174133, 10 p.
Sondergeld, C.H., Newsham, K.E., Comisky, J.T., Rice, M.C., Rai, C.S., 2010. Petrophysical considerations in evaluating and producing shale gas resources. In: SPE Unconventional Gas Conference. Society of Petroleum Engineers, Pittsburgh, Pennsylvania, USA, February 23 – 25, 2010, SPE Paper 131768, 34 p.
Sone, H., Zoback, M.D., 2013a. Mechanical properties of shale-gas reservoir rocks—Part 1: Static and dynamic elastic properties and anisotropy. Geophysics 78, D381–D392.
Sone, H., Zoback, M.D., 2013b. Mechanical properties of shale-gas reservoir rocks—Part 2: Ductile creep, brittle strength, and their relation to the elastic modulus. Geophysics 78, D393–D402.
Stewart, C.J., 2017. Stratigraphic and Petrographic Analysis of the Late Devonian-Early Mississippian Lower and Upper Bakken Shale Members for the Development of a Sequence Stratigraphic Framework (Master thesis). Indiana University, Bloomington 115 p.
Strąpoć, D., Mastalerz, M., Schimmelmann, A., Drobniak, A., Hasenmueller, N.R., 2010. Geochemical constraints on the origin and volume of gas in the New Albany Shale (Devonian–Mississippian), eastern Illinois Basin. AAPG Bull. 94, 1713–1740.
Swezey, C.S., 2007. Assessment of undiscovered oil and gas resources of the Illinois Basin. U.S. Geol. Surv Fact Sheet 2007–3058, 2 p.
Thyberg, B., Jahren, J., 2011. Quartz cementation in mudstones: sheet-like quartz cement from clay mineral reactions during burial. Pet. Geosci. 17, 53–63.
Thyberg, B., Jahren, J., Winje, T., Bjørlykke, K., Faleide, J.I., Marcussen, Ø., 2010. Quartz cementation in Late Cretaceous mudstones, northern North Sea: Changes in rock properties due to dissolution of smectite and precipitation of micro-quartz crystals. Mar. Pet. Geol. 27, 1752–1764.
Walles, F., 2004. A new method to help identify unconventional targets for exploration and development through integrative analysis of clastic rock property fields. Houston Geol. Soc. Bull. 47, 35–36.
Wang, F.P., 2008. Production fairway: Speed rails in gas shale? In: The 7th Annual Gas Shales Summit. Dallas, Texas, USA, May 6–7, 2008.
Wang, F.P., Gale, J.F., 2009. Screening criteria for shale-gas systems. Gulf Coast Assoc. Geol. Soc. 59, 779–793.
Xu, J., Sonnenberg, S., 2016. Brittleness and rock strength of the Bakken Formation, Williston Basin, North Dakota. In: Unconventional Resources Technology Conference. SPE-AAPG-SEG, San Antonio, Texas, August 1 – 3, 2016, Paper 2460490, 18 p.
Yang, J., Hatcherian, J., Hackley, P.C., Pomerantz, A.E., 2017. Nanoscale geochemical and geomechanical characterization of organic matter in shale. Nat. Commun. 8, 2179.
Yang, S., Harris, N., Dong, T., Wu, W., Chen, Z., 2015. Mechanical Properties and Natural Fractures in a Horn River Shale Core from Well Logs and Hardness Measurements. Society of Petroleum Engineers, Madrid, Spain, June 1–4, 2015, SPE Paper 174287. 13 p.
Ylagan, R.F., Altaner, S.P., Pozzuoli, A., 2000. Reaction mechanisms of smectite illitization associated with hydrothermal alteration from Ponza Island, Italy. Clay Clay Miner. 48, 610–631.
Zargari, S., Prasad, M., Mba, K.C., Mattson, E.D., 2013. Organic maturity, elastic properties, and textural characteristics of self resourcing reservoirs. Geophysics 78, D223–D235.
Zhang, C., Dong, D., Wang, Y., Guan, Q., 2017. Brittleness evaluation of the Upper Ordovician Wufeng–Lower Silurian Longmaxi shale in Southern Sichuan Basin, China. Energy Explor. Exploit. 35, 430–443.
Zhao, J., Jin, Z., Jin, Z., Wen, X., Geng, Y., 2017. Origin of authigenic quartz in organic-rich shales of the Wufeng and Longmaxi Formations in the Sichuan Basin, South China: Implications for pore evolution. J. Nat. Gas Sci. Eng. 38, 21–38.